Growth and characterization of PbI_2-decorated ZnO nanowires for photodetection applications

Edgars Butanovs *, Sergei Piskunov , Aleksejs Zolotarjovs , Boris Polyakov

Institute of Solid State Physics, University of Latvia, Kengaraga Street 8, Riga, LV-1063, Latvia

a b s t r a c t

In this study, we demonstrated for the first time the growth of ZnO nanowires (NWs) decorated with highly crystalline few-layer PbI_2 and fabricated two-terminal single-nanowire photodetector devices to investigate the photoelectric properties of the hybrid nanostructures. We developed a novel two-step growth process for uniform crystalline PbI_2 nanosheets via reactive magnetron deposition of a lead oxide film followed by subsequent iodination to PbI_2 on a ZnO NW substrate, and we compared as-grown hybrid nanostructures with ones prepared via thermal evaporation method. ZnO$e$$PbI_2$ NWs were characterized by scanning and transmission electron microscopy, X-ray diffraction analysis and photo-luminescence measurements. By fabricating two-terminal single-nanowire photodetectors of the as-grown ZnO$e$$PbI_2$ nanostructures, we showed that they exhibit reduced dark current and decreased photoresponse time in comparison to pure ZnO NWs and have responsivity up to 0.6 A/W. Ab initio calculations of the electronic structure of both PbI_2 nanosheets and ZnO NWs have been performed, and show potential for photoelectrocatalytic hydrogen production. The obtained results show the benefits of combining layered van der Waals materials with semiconducting NWs to create novel nanostructures with enhanced properties for applications in optoelectronics or X-ray detectors.

1. Introduction

The surface plays an exceptionally important role in deter-mining nanomaterial physical and chemical properties. The impact of surface modification on nanoscale material properties has been intensively explored for the last few decades [1e3]. Nanowires (NWs) are one-dimensional (1D) nanomaterials that exhibit promising properties beneficial for integration in functional de-vices, such as photodetectors, nanolasers, LEDs, etc. [4,5], and modification of their surface can significantly improve their elec-trical, optical and mechanical characteristics [3,4,6]. Modification or decoration of a NW surface has no restrictions of material lattice mismatch and its caused stress at the interface, unlike the con-ventional thin film growth [5,7,8], therefore, opening new possi-bilities to engineer novel hybrid nanostructures with desired properties, such as photon detection capability in a broad spectral range [9]. Currently, most research in this field is focused on developing precisely controllable nanostructure fabrication methods and tuning nanostructure properties for specific applica-tions [6,7,9].

Zinc oxide (ZnO) is one of the most commonly studied NW materials due to its simple synthesis and wide field of applications, such as ultraviolet photodetectors [10,11] and piezoelectric nano-generators [12], as well as the potential to be a scintillator material for X-ray detectors [13e15]. ZnO is an n-type semiconductor with a direct bandgap around 3.2e3.4 eV and it has a high exciton binding energy (60 meV), which allows room temperature excitonic emis-sion [16]. ZnO NWs have frequently been used as template material for nanomaterial synthesis [17,18]. Furthermore, in several studies, it has been demonstrated that passivating the surface of ZnO nanostructures or decorating the NWs with specifically selected materials enhances light and gas detecting properties [19e24].

Lead (II) iodide (PbI_2) is a photoconductor material with 2.2e2.55 eV bandgap [25] and is typically employed in fabricating perovskite solar cells and photodetectors [26e30], and as an X-ray and g-ray detector material [31e34]. PbI_2 has a layered structure in which the covalently bonded IePbeI repeating layers are bound by weak van der Waals (vdW) interaction [35]. Recently, it has gained more attention due to the extensive research on various 2D vdW materials, such as graphene and transition metal dichalcogenides

[36,37]. There are theoretical and experimental studies that show band structure shift from direct bandgap to indirect bandgap when the PbI_2 thickness is reduced from bulk to monolayer [35,38], as opposed to well-studied vdW materials, MoS_2, for example [39]. Therefore, monolayer PbI_2 is not expected to be an efficient mate-rial for optoelectronics applications. In the last few years, there have been several studies that demonstrate the growth of few-layer PbI_2 crystals and investigate their promising photodetection properties both on rigid and flexible substrates [25,35,40e42]. The growth of 1D PbI_2 NWs for high-sensitivity photodetector appli-cations has also been reported [43]. Zhang et al. proposed low-temperature heteroepitaxial growth of PbI_2 thin film on submeter-sized graphene/polyethylene terephthalate (PET) sub-strate and showed its applicability in light detection [44]. However, there are challenges remaining in obtaining highly-crystalline and uniform large-area PbI_2 films.

Alternatively, NWs can be used as a template for growth and easier manipulation of layered vdW materials, such as WS_2 and MoS_2, while maintaining the high crystallinity of the materials used and even enhancing their properties [20,45e47]. Large-scale printing of NWs at specified locations on flexible substrates via roll-to-roll transfer has been demonstrated [48], therefore enabling the advancement of all-printed layered material- and NW-based electronic and optoelectronic devices in the future. Furthermore, some research has been done on the development of high-resolution NW-arrays for X-ray imaging [49,50]. There are also few reports on using single-nanowire devices for X-ray detection and beam shape characterization [51e53]. Consequently, using ZnO and PbI_2 materials in 1D hybrid nanostructures could potentially lead to next-generation high-resolution direct-conversion digital X-ray detector devices with advanced properties.

In this work, we demonstrate two different approaches to syn-thesise novel 1D ZnOePbI2 nanostructures. Highly crystalline few-layer PbI_2 was grown on ZnO NWs by: (1) direct thermal evapo-ration of PbI_2 powder, and (2) the conversion of a sputter-deposited lead oxide coating in iodine vapour at an elevated temperature. Two-terminal single-nanowire photodetectors were fabricated to show their enhanced photoelectric properties compared to pure ZnO NWs. The results show the potential of combining layered vdW materials with semiconducting nanowires to create novel nano-structures with advanced properties for potential photodetection applications. From our ab initio modelling, nanosized ZnOePbI2 heterostructures might be used for efficient photocatalytic hydrogen production from water.

2. Experimental details

2.1. Nanostructure synthesis and characterization

ZnO NWs were synthesised on oxidized silicon wafers SiO_2/ Si(100) (Semiconductor Wafer, Inc.) via atmospheric pressure chemical vapour transport in an open-end horizontal quartz tube reactor using spherical Au nanoparticles (Smart materials, water suspension, 100 nm diameter) as a catalyst for the vapour-liquid-solid mechanism [54]. In short, 0.5 g of a 1:1 mixture of ZnO and carbon powders was loaded in a ceramic boat in the centre of the quartz tube at 900 C. The vapour was transported downstream to the Au/Si substrate at a lower temperature region using N_2 as a carrier gas. The temperature was held constant for 90 min, followed by natural cooling to the room temperature. See Fig. S1 for the scanning electron microscope (SEM) images and X-ray diffraction (XRD) pattern of the as-grown ZnO NWs.

In the next step, a few layers of PbI_2 were deposited on the as-grown ZnO NW arrays via two different approaches: (1) thermal evaporation of a PbI_2 powder and (2) sputter deposition of a lead oxide coating followed by iodination at elevated temperatures. Both evaporation and sputtering were carried out in a Sidrabe SAF25/50 multifunctional cluster tool. In the first method, a simple thermal evaporation process was carried out in a vacuum chamber at 10^{-5} torr while rotating the ZnO NW sample (60 mg PbI_2 powder was evaporated from an Al_2O_3 crucible). The second method con-sists of two steps. First, a lead oxide PbO_x coating (consisting of different phases, including PbO and PbO_2 as shown by the XRD data in Fig. S2) was obtained by reactive DC magnetron sputtering of a metallic lead target in a mixed Ar/O_2 atmosphere (20$10^{-3}$ torr, 20 sccm Ar and 10 sccm O_2 gas flows, 5 min of sputtering at 100 W DC power). Second, as-prepared ZnO-PbO_x samples were annealed in a quartz tube in an iodine atmosphere for 15 min using an Ar/H_2 5% mixture as the carrier gas to convert lead oxide to lead iodide. An iodine-rich atmosphere was obtained by placing 0.25 g iodine powder upstream of the sample at 120 C. The optimal annealing temperature was found to be 420 C, and the lead oxide conversion to PbI_2 starts around 350 C. One must optimize between a high coating crystallinity and the sublimation rate of the converted PbI_2 film, which increases rapidly above 400 C. As a reference sample for comparison, a PbI_2 thin film on SiO_2/Si substrate was prepared using the second approach.

The as-prepared nanostructure morphology was characterized using SEM-FIB (Lyra, Tescan), while the crystalline structure of the PbI_2 coating and ZnO NW was using a transmission electron mi-croscope (TEM, Tecnai GF20, FEI) operated at a 200 kV accelerating voltage. The phase composition of the samples was studied using XRD (q-q Bragg Brentano powder diffractometer PANalytical X'Pert Pro) with monochromatic Cu Ka irradiation and the spectra were analysed using PDXL2 software. Room-temperature photo-luminescence (PL, Hamamatsu R92P PMT) spectra with a 266 nm excitation wavelength (fourth harmonic of CryLas Nd:YAG laser, 0.3 mJ power, 1 ns pulse duration, 5 kHz repetition rate) were measured to investigate the as-prepared nanostructure optical properties.

2.2. Single nanowire two-terminal photodetector device fabrication

To fabricate two-terminal single-nanowire photodetectors, first, gold microelectrodes with a 2 mm gap width were prepared on an oxidized silicon wafer by a conventional photolithography tech-nique (see Fig. S3). The microelectrode array pattern was obtained using direct-write laser lithography (mPG101, Heidelberg In-struments) on Megaposit SPR700 photoresist (Rohm and Haas Electronic Materials), 5/45 nm Cr/Au film was deposited via thermal evaporation method followed by a lift-off procedure. Second, NWs were transferred onto the electrode array by mechanically pressing it to the substrate with the as-grown nanostructures, followed by welding selected single NWs to the corresponding underlying gold microelectrodes using electron-beam-assisted platinum deposition inside SEM-FIB to ensure the electric contact and fixed position. At least ten single-nanowire photodetectors (more than five for each synthesis method) were fabricated so consistent conclusions could be made.

2.3. Device measurements

Current voltage (IeV) characteristics and photoresponse of the fabricated single-NW photodetector devices were measured with a two-contact microprobe station connected to a low-noise current preamplifier (SR570, Stanford Research Systems) and oscilloscope (TDS2004B, Tektronix). A 405 nm wavelength semiconductor diode laser (CNI Laser) with 1 W/cm^2 power was the illumination source for the photoresponse measurements. An optical beam shutter (Thorlabs SH05) was used for time-resolved measurements. All the

measurements were performed at room temperature and in air.

2.4. Computational details

Total energy first-principle calculations for [0001]-oriented mono- (ML), bi- (2 ML) and three-layered (3 ML) PbI_2 nanosheets, and 24-layer thick [1e100] oriented slabs, to mimic the surface of ZnO nanowires, were performed using the HSE06 hybrid exchange-correlational functional [55] within the density functional theory (DFT), as implemented in the computer code CRYSTAL17 [56]. Localized Gaussian type functions (GTFs) in the form of atom-centred basis sets (BSs) for expansion of periodic crystalline or-bitals for Zn and O were taken in the form of full electron Triple-Zeta Valence BS with polarization functions [56], while effective-core pseudopotential BS were taken for Pb and I [56]. The reli-ability of the chosen theoretical method were proven by calcula-tions of bandgap energy (d) for bulk phase ZnO and PbI_2 crystals (see Fig. S5). The calculated bandgaps for all materials under study are in good agreement with those experimentally observed. To provide a balanced summation in both direct and reciprocal lat-tices, reciprocal space integration was performed by sampling the Brillouin zone (BZ) with a 6 6 1 Pack-Monkhorst mesh [57], which results in a total of 20 k-points evenly distributed over the BZs. For every fixed crystalline geometry calculation, the conver-gency was reached only when the total energy differed by less than

10^{7} a.u. in two successive cycles of the self-consistent field (SCF) procedure [56]. Full geometry optimization was performed for all nanostructures considered in this study.

3. Results and discussion

3.1. Morphology, structure and photoluminescence measurements

SEM was used to image as-grown individual NWs and NW ar-rays and study their morphology. Pure ZnO NWs are typically 20e30 mm long with a diameter around 100 nm and exhibit a smooth surface (see Figs. S1(a and b)). Fig. 1(a and b) shows ZnO NWs with a thermally deposited PbI_2 coating. No significant change in diameter is observed; however, a very fine increase in surface roughness is visible. NWs with a sputter-deposited lead oxide coating with a fine roughness are shown in Fig. 1(c and d), where a considerable (up to 100 nm) increase in diameter can be seen. After annealing such NWs in iodine vapour at elevated temperatures, the surface roughness greatly increased; however the diameter is significantly reduced as a fraction of the coated material is subli-mated after the transformation (see Fig. 1(e and f)). The final coating is not uniform over the entire length of NWs as some thicker particles and islands can be observed. SEM images of the reference sample, PbI_2 thin film converted from sputter-deposited lead oxide, are shown in Fig. 1(g and h). The film exhibits hexago-nal domains, presumably highly crystalline as PbI_2 typically crys-tallizes in a hexagonal structure.

A deeper insight into the nanostructures' inner structure was obtained using TEM. Fig. 2(aec) shows TEM images of ZnOePbI$_2$ NWs obtained by the thermal evaporation method at different magnifications. The lower resolution images show noticeable contrast between the two NW sides (PbI_2 layers correspond to the darker region), indicating non-uniform coating deposition, which is expected from the thermal evaporation approach since it is a line-of-sight method. At a high resolution, the crystalline structure of the nanostructure is revealed. The layers of PbI_2 grown on the ZnO NW surface are distinguishable as parallel black lines. Typically, the thickness of the coating varies between 5 and 10 monolayers (each consisting of IePbeI atomic planes), with interlayer distance measured around 7 Å, which is in a good agreement with the lattice constant (a ¼ 6.979 Å) of bulk hexagonal PbI_2 (ICDD-PDF #07e0235). Furthermore, the single-crystalline nature of the ZnO NWs is clearly visible; the measured interplanar distance is 2.8 Å, corresponding to hexagonal ZnO wurtzite (ICDD-PDF #36e1451), as confirmed by the XRD pattern (see Fig. S1(c)). The TEM images of the ZnOePbI$_2$ nanostructures obtained by conversion of sputter-deposited lead oxide coating are shown in Fig. 2(def). In this case, the PbI_2 coating is uniformly distributed over the entire ZnO NW surface; however, the surface roughness is significantly increased. The thickness of the coating typically varies between 5 and 15 monolayers, with some islands being even thicker. As in to the first approach, the measured interlayer distance is around 7 Å.

To complement TEM structural investigations and confirm the presence of phases, XRD measurements were performed on the as-prepared samples. Fig. 3(a and b) show XRD patterns of NW arrays prepared by the two approaches: thermal evaporation and con-verting the magnetron-sputtered lead oxide coating, respectively.

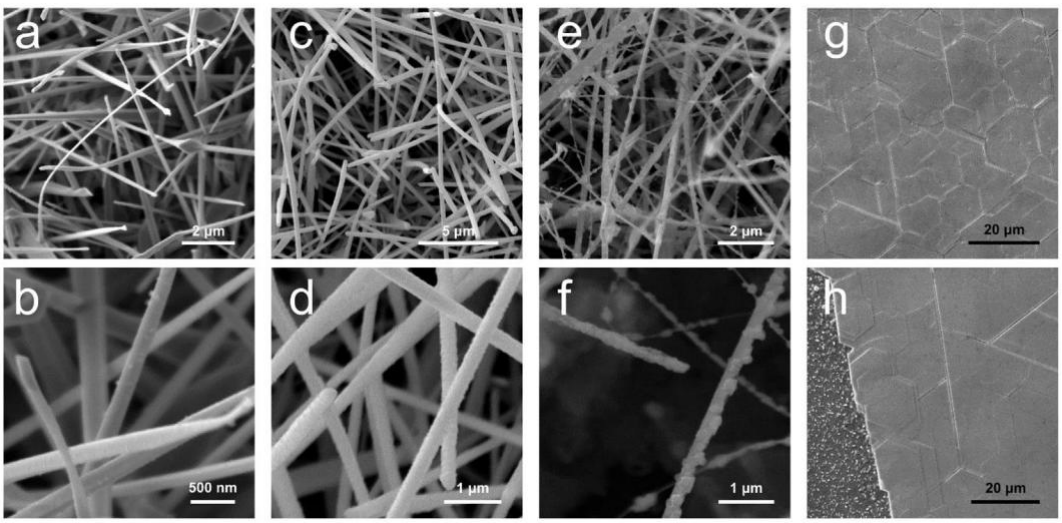

Fig. 1. Scanning electron microscope images of (a,b) ZnOePbI$_2$ NWs made using the thermal evaporation approach; (c,d) ZnO NWs covered by lead oxide deposited by magnetron sputtering; (e,f) ZnOePbI$_2$ NWs made by converting the lead oxide coating; (g,h) PbI_2 thin film made by converting a lead oxide film.

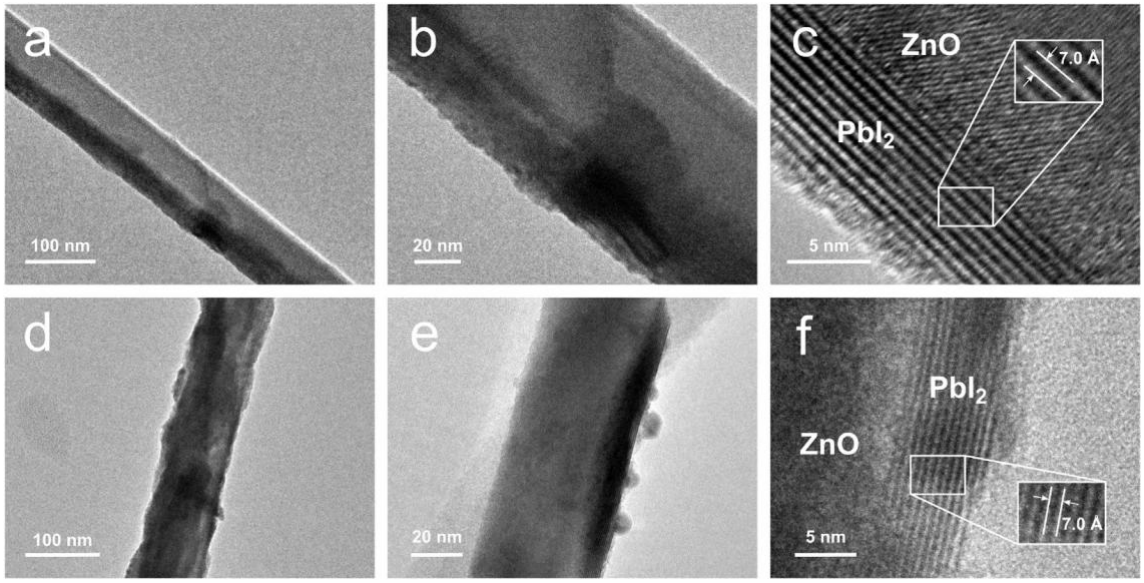

Fig. 2. Transmission electron microscope images at different magnifications of (a,b,c) ZnOePbI2 NWs made using the thermal evaporation approach, and (d,e,f) ZnOePbI2 NWs made by converting the magnetron-sputtered lead oxide coating. The insets show measured atomic interlayer distances between PbI2 layers.

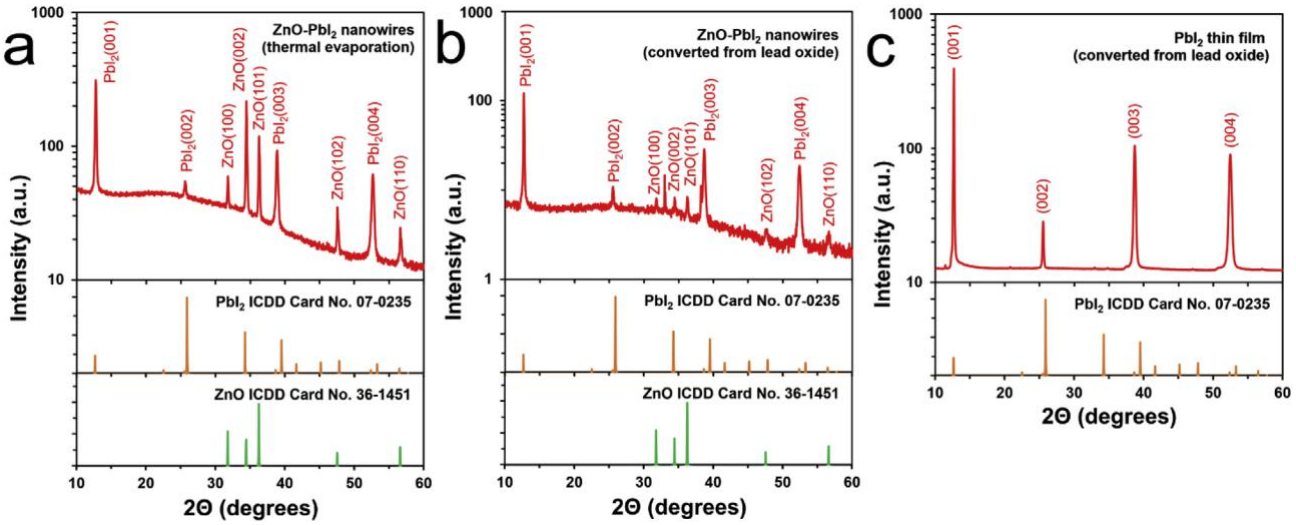

Fig. 3. X-ray diffraction patterns of (a) ZnOePbI2 NW arrays on Si/SiO2 substrate made using the thermal evaporation approach; (b) ZnOePbI2 NW arrays on Si/SiO2 substrate made by converting the magnetron-sputtered lead oxide coating; (c) PbI2 thin film made by converting a lead oxide film.

Both patterns indicate highly crystalline hexagonal ZnO wurtzite (ICDD-PDF #36e1451) and hexagonal PbI2 (ICDD-PDF #07e0235) phases. No other phases were observed, confirming the high crys-tallinity of the as-prepared nanostructures, as did the TEM in-vestigations. It is worth noting that the ratio between PbI2 and ZnO peak intensity is not only related to the amount of PbI2 on ZnO NWs but also the amount of PbI2 crystallites on the Si/SiO2 substrate. Therefore, spectra cannot be properly used to describe the phase composition ratio in the nanostructures. Furthermore, ZnO NW Bragg peak intensities vary between the samples - due to an inhomogeneous gold nanoparticle catalyst deposition from colloid on the silicon substrate; the density of as-grown ZnO nanowires arrays was also not homogeneous while the PbI2 layer is relatively homogeneous over the substrate due to the precisely controllable deposition method. In Fig. 3(b), the Bragg peak at 33 is attributed to diffraction in the Si(100) substrate (forbidden Si(200) reflection).

The XRD pattern of pure ZnO NWs is given in Fig. S1(c). The XRD pattern of the PbI2 thin film reference sample shows its highly crystalline structure (see Fig. 3(c)), confirming that the conversion of a lead oxide film in iodine vapour is a viable method how to obtain crystalline PbI2 thin films.

To study the optical properties, room temperature PL in the as-prepared samples was measured in a wavelength range from 400 to 650 nm, excited by a 266 nm laser. Generally, PbI2 has a direct band-to-band transition at around 495 nm (~2.5 eV) [58]; however, a broad band peaked at 510e525 nm has been previously observed and attributed to recombination through defects, such as iodine and lead vacancies [25]. The PL spectrum of pure ZnO NWs exhibits a defect-related band at ~520 nm [16]. Therefore, the interpretation of the ZnOePbI2 nanostructure spectra might be ambiguous due to this ZnO and PbI2 PL band overlapping, since higher ZnO PL in-tensities might lead to indistinguishable PbI2 PL peaks or vice versa.

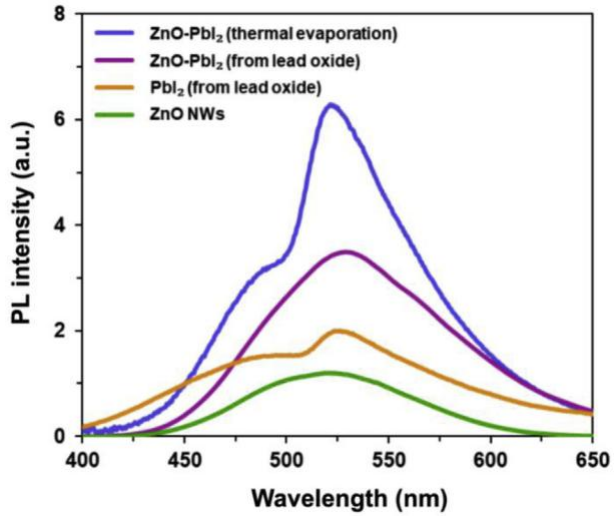

Fig. 4. Room temperature photoluminescence (PL) spectra at 266 nm excitation wavelength for the different as-prepared samples. The PL intensity is depicted in arbitrary units and does not contain information about relative intensities between the measured spectra.

Fig. 4 depicts our measured PL spectra of pure ZnO NWs, the PbI_2 thin film reference sample, and the ZnO–PbI_2 nanostructures prepared via both approaches. It is worth noting that the PL in-tensity is depicted in arbitrary units and does not contain infor-mation about the relative intensities between the obtained spectra. The ZnO NW spectrum exhibits the typical defect band at 520 nm and the PbI_2 thin film sample (prepared by converting lead oxide film) shows two emission peaks: the direct band-to-band transition at around 495 nm and the defect-related band at around 530 nm. The ZnO–PbI_2 nanostructures (prepared by thermal evaporation approach) exhibit two peaks at 495 nm and 525 nm; however, the nanostructures prepared via lead oxide conversion exhibit only one band with a peak at 530 nm due to the higher intensity overlapping ZnO peak. One can see and interpret the difference between the PbI_2 peak ratio for samples prepared with different methods due to the defect-related peak maximum shift. For example, the defect/ band-to-band peak intensity ratio for thermally evaporated PbI_2 is ~2, while for lead oxide converted PbI_2, it is ~1.33 Therefore, by also considering the ZnO peak contribution, one can qualitatively assume that lead oxide conversion via iodination leads to fewer defects in PbI_2 coatings than the thermal evaporation approach.

3.2. Device photoresponse measurements

Two-terminal single-nanowire photodetectors were fabri-cated from the nanostructures prepared via both approaches, and pure ZnO NWs. Fig. 5(aec) shows the characteristics of the ZnO–PbI_2 single NW devices made using the thermal evaporation approach, while Fig. 5(def) shows the characteristics of the ZnO–PbI_2 single NW devices made by converting the magnetron-sputtered lead oxide coating (more than five single-nanowire photodetectors for each synthesis method were fabricated so that consistent conclusions could be made). The inset contains an SEM image of a typical as-prepared NW device. Both dark state current-voltage (IeV) characteristics of ZnO–PbI_2 NWs in Fig. 5(a) and (d) exhibit linear behaviour, indicating that ohmic contacts formed between the nanostructures and the electrodes, as is expected for PbI_2 on gold [40,59] and which is beneficial for efficient photogenerated carrier collection. In contrast, pure ZnO NWs typically form Schottky contact with gold electrodes (see the nonsymmetric IeV curve in Fig. S4(a)) [60]. The devices were illuminated with 405 nm wavelength light in a periodic fashion to study their photoresponse properties as shown in Fig. 5(b) and (e). All the devices were also tested for 532 nm and 660 nm light

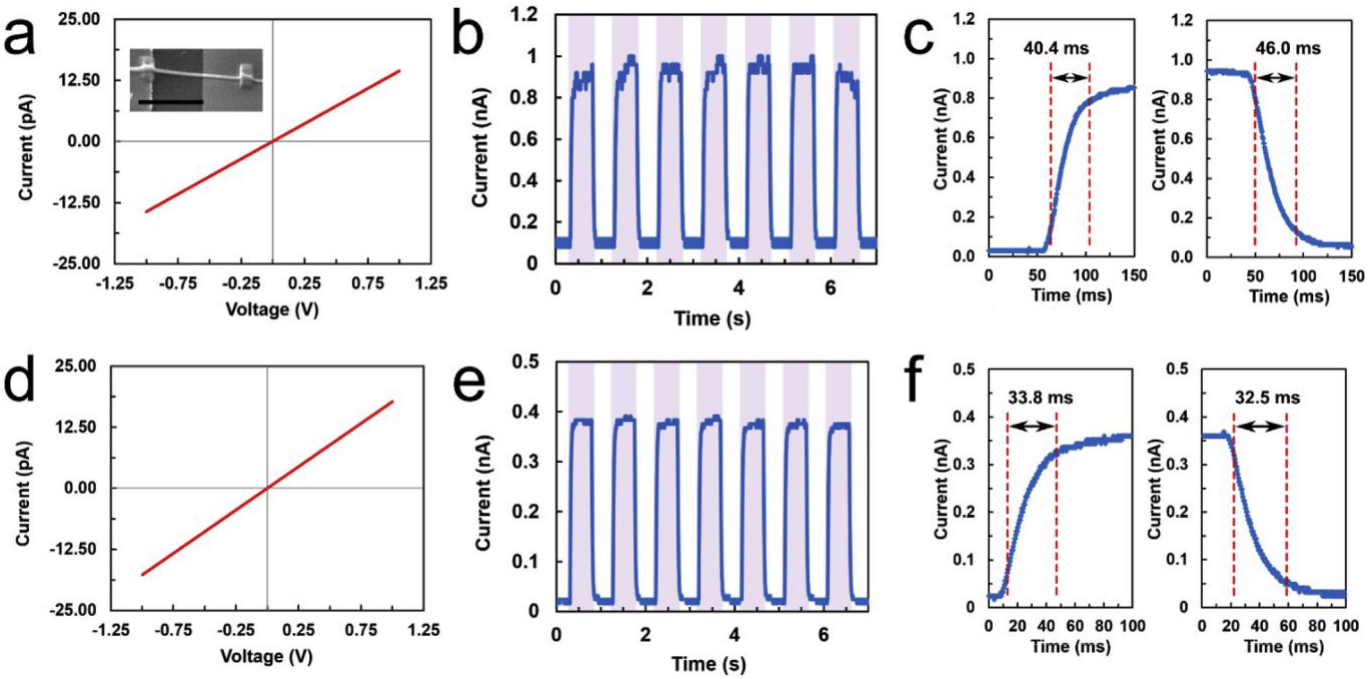

Fig. 5. ZnO–PbI_2 single NW made using the thermal evaporation approach (a) dark state IeV characteristics, (b) on off photoresponse, (c) time-resolved photoresponse mea-surements; and ZnO–PbI_2 single NW made by converting the lead oxide coating (d) dark state IeV characteristics, (e) on off photoresponse, (f) time-resolved photoresponse measurements at 1 V bias voltage and 1 W/cm^2 light intensity with 405 nm wavelength light. The inset shows an SEM image of a typical single-nanowire two-terminal photo-detector. The scale bar corresponds to 2 mm.

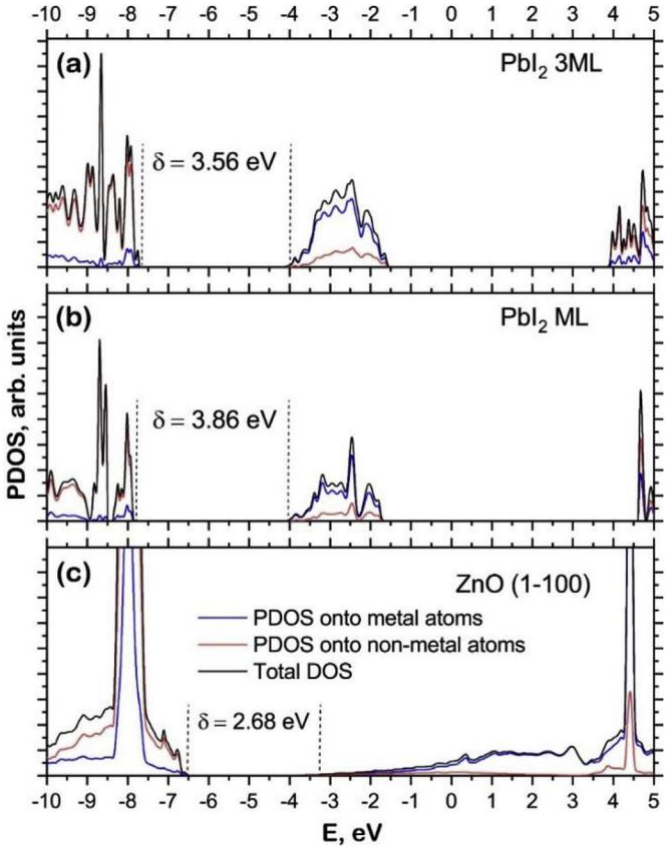

Fig. 6. Total and projected densities of states (PDOS) calculated for (a) 3-monolayer thick PbI_2 nanosheet, (b) monolayer thick PbI_2 nanosheet, and (c) ZnO (1e100) slab. The 24-layer thick slab of ZnO substrate is symmetrically terminated to mimic the surface of the nanowires. PDOS projected onto all orbitals of corresponding metal or non-metal atoms. The energy scale is shown with respect to the vacuum level.

illumination; however, no increase in current was observed due to the relatively wide bandgap of the studied materials. On-off measurements demonstrate a steady, rapid and repeatable in-crease and decrease of the current when the illumination is turned on or off, respectively; therefore, showing good stability and reversibility of the devices. ZnOePbI2 NWs exhibit low dark current (10e100 pA) which is necessary for high-performance photodetectors, while for pure ZnO NWs, it can be up to several tens of nA (see Fig. S4(b)). The current enhancement ratios (I_{on}/ I_{off}) for the nanostructures prepared via both approaches were measured to be at around 10e20, in contrast to less than 2 for pure ZnO NWs. Time-resolved photoresponse measurements were performed to evaluate the rise and decay time of the as-prepared ZnOePbI2 devices, defined as the required time for the photocurrent to increase or decrease to 90% or 10% of its maximum value, respectively. As shown in Fig. 5(c) and (f), the obtained values are in the 30e50 ms range, which is almost two orders of magnitude faster than the pure ZnO NWs (see Fig. S4(c)) and comparable to typical NW or 2D PbI_2 photodetector response times [35,41,42,59,61]. The slow response of ZnO NWs is due to the influence of oxygen molecules on the surface states and their effect on photoresponse kinetics is widely discussed in the liter-ature [62,63]. Here and in our previous work [20], we passivated the surface of ZnO NWs using a thin PbI_2 or WS_2 coating, respectively, and photodetectors of such heterostructures exhibit reduced dark current and photoresponse time, although it also decreased on-state current I_{on} in comparison to pure ZnO NWs. It is well known that adsorbed oxygen species influence electrical properties (electrical conductivity decreases with exposure to oxygen) of metal oxide nanostructures [11,64e66]. Consequently, band bending, induced by adsorbed oxygen molecules that cap-ture free electrons, causes an efficient photogenerated electron-hole separation that leads to high gain in single-nanowire pho-todetectors. The presence of the PbI_2 layers in our nanostructures protects the ZnO surface from oxygen adsorption that might in-fluence surface-related photoinduced processes and decrease the number of charge carrier trapping centres.

The thickness of PbI_2 on ZnO NWs, which were used in the as-fabricated photodetector devices, was typically 6e13 layers. No significant changes in the photodetector characteristics, such as spectral responsivity R|, response time or current enhancement ratios (I_{on}/I_{off}), were observed between the samples in this PbI_2 thickness range. It is worth noting, that there are theoretical and experimental studies that show a band structure shift from direct bandgap to indirect bandgap when the PbI_2 thickness is reduced from bulk to monolayer [35,38]; therefore, monolayer PbI_2 is not expected to be an efficient material for optoelectronics applications and few-layer PbI_2 should be used instead.

Spectral responsivity (R|) and external quantum efficiency (EQE) are used to evaluate photoconductive properties of a mate-rial. R| and EQE are respectively defined as R| ¼ DI/(PS) and EQE ¼ hcR|/(el) [40], where DI is the difference between the photocurrent I_{on} and the dark current I_{off}, P is the light power density, S is the effective illumination area (estimated as the elec-trode gap width NW diameter), h is Planck's constant, c is the speed of light, e is the electron charge and l is the light wavelength. Large R| and EQE values correspond to high photodetector sensi-tivity. A responsivity as high as ~0.6 A/W (EQE ~180%) was calcu-lated for the ZnOePbI2 single NW devices made using the thermal evaporation approach and ~0.3 A/W (EQE ~90%) for the ones made by converting the magnetron-sputtered lead oxide coating; how-ever, it is not valid to compare the two different synthesis ap-proaches based only on the responsivity values as the value range for all as-fabricated devices overlapped no matter which method was used. The obtained R| and EQE values are comparable to other typical state-of-the-art 1D nanostructure [61] and 2D PbI_2 [41,42,44,59] photodetectors.

3.3. Electronic structure calculations

Fig. 6 compares the total and projected densities of states (PDOS) calculated for [0001]-oriented monolayered (ML) and three-layered (3 ML) PbI_2 nanosheets, Fig. 6(a) and (b), respectively, and the PDOS calculated for slab models of [1e100] oriented ZnO NW (Fig. 6(c)). The PDOS calculated for bi-layered (2 ML) PbI_2 nanosheet is not presented in Fig. 6 since its electronic structure does not practically differ from that calculated for 3 ML PbI_2. For all PbI_2 nanosheets under study, the upper part of the valence band (VB) is predominantly formed by the iodine (5p) orbitals with significant contributions from lead (6s) orbitals. The bottom of the conduction band (CB) of PbI_2 nanosheets is formed mainly from Pb (6p) states. In the case of ZnO (1e100) surfaces, the VB top is formed by oxygen 2p states, while 3d orbitals of Zn mainly form the CB bottom. The band edge positions of ML and 3 ML PbI_2 differ from those of bulk (Fig. S5(a)). The bottom of the CB is shifted down, closer to the hydrogen evolution potential of 4.44 eV. The position of the top of the VB calculated for (1e100) ZnO NW surfaces is located near 5.67 eV oxygen reduction potential, which allows us to conclude that the hybrid ZnOePbI2 NWs can be considered as promising potential materials for efficient solar-driven photo (electro)catalytic water splitting.

4. Conclusions

In this paper, we demonstrated for the first time the growth of ZnO NWs decorated with highly crystalline few-layer PbI_2 and fabricated two-terminal single-nanowire photodetector devices to investigate the photoelectric properties of the hybrid ZnO–PbI_2 nanostructures. We developed a novel two-step growth process for uniform crystalline PbI_2 nanosheets via reactive magnetron depo-sition of a lead oxide film followed by subsequent iodination in iodine vapour to PbI_2 at 420 C on a ZnO NW substrate, and we compared as-grown hybrid nanostructures with ones prepared via thermal evaporation method. As-prepared two-terminal single-nanowire ZnO–PbI_2 photodetectors are comparable to state-of-the-art 1D nanostructure and 2D PbI_2 photodetectors and exhibit enhanced optoelectronic characteristics, such as reduced dark current and significantly decreased photoresponse time compared to pure ZnO NWs, and have responsivity up to 0.6 A/W. We found that the preparation method does not significantly affect the pho-toelectric properties of the nanostructures; however, PbI_2 obtained by thermal evaporation benefits from a smoother coating and, presumably, less optical defect states, but lacks the uniform coverage of PbI_2 converted from lead oxide coating. First principle DFT calculations on few-layer PbI_2 nanosheets, thin slabs to mimic the surface of ZnO NWs, and bulk phase ZnO and PbI_2 crystals, were performed to obtain the electronic structure of the materials under study. The results show the potential of combining layered vdW materials with semiconducting nanowires to create novel nano-structures with enhanced properties for applications in optoelec-tronics or X-ray detectors. Our ab initio modelling also shows that nanosized ZnO–PbI_2 heterostructures might be used for efficient photocatalytic and electrocatalytic hydrogen production from water.

Declaration of competing interest

There are no conflicts of interest to declare.

CRediT authorship contribution statement

Edgars Butanovs: Methodology, Validation, Investigation, Visualization, Writing - original draft. Sergei Piskunov: Method-ology, Formal analysis, Visualization. Aleksejs Zolotarjovs: Inves-tigation. Boris Polyakov: Conceptualization, Supervision, Investigation, Writing - review & editing.

Acknowledgements

Financial support provided by Scientific Research Project for Students and Young Researchers Nr. SJZ/2017/1 realized at the Institute of Solid State Physics, University of Latvia is greatly acknowledged. The authors are grateful to Liga Bikse for XRD measurements.

References

[1] J. Wen, et al., Photocatalysis fundamentals and surface modification of TiO2 nanomaterials, Chin. J. Catal. 36 (2015) 2049e2070.
[2] Y. Guo, K. Xu, C. Wu, J. Zhao, Y. Xie, Surface chemical-modification for engi-neering the intrinsic physical properties of inorganic two-dimensional nanomaterials, Chem. Soc. Rev. 44 (2015) 637e646.
[3] A. Pescaglini, D. Iacopino, Metal nanoparticleesemiconductor nanowire hybrid nanostructures for plasmon-enhanced optoelectronics and sensing, J. Mater. Chem. C 3 (2015) 11785e11800.
[4] R. Yan, D. Gargas, P. Yang, Nanowire photonics, Nat. Photon. 3 (2009) 569e576.
[5] Y. Li, F. Qian, J. Xiang, C.M. Lieber, Nanowire electronic and optoelectronic devices, Mater. Today 9 (2006) 18e27.
[6] L.J. Lauhon, M.S. Gudiksen, D. Wang, C.M. Lieber, Epitaxial coreeshell and coreemultishell nanowire heterostructures, Nature 420 (2002) 57e61.
[7] Y. Dong, B. Tian, T.J. Kempa, C.M. Lieber, Coaxial group III Nitride nanowire photovoltaics, Nano Lett. 9 (2009) 2183e2187.
[8] T.J. Kempa, R.W. Day, S.-K. Kim, H.-G. Park, C.M. Lieber, Semiconductor nanowires: a platform for exploring limits and concepts for nano-enabled solar cells, Energy Environ. Sci. 6 (2013) 719.
[9] W. Tian, D. Liu, F. Cao, L. Li, Hybrid nanostructures for photodetectors, Adv. Opt. Mater. 5 (2017) 1600468.
[10] Y. Zhang, M.K. Ram, E.K. Stefanakos, D.Y. Goswami, Synthesis, characteriza-tion, and applications of ZnO nanowires, J. Nanomater. 1e22 (2012), 2012.
[11] C. Soci, et al., ZnO nanowire UV photodetectors with high internal gain, Nano Lett. 7 (2007) 1003e1009.
[12] Z.L. Wang, Piezoelectric nanogenerators based on zinc oxide nanowire arrays, Science 312 (2006) 242e246.
[13] M.J.F. Empizo, et al., Photoluminescence properties of a single ZnO micro-structure for potential scintillator applications, Opt. Mater. (Amst). 38 (2014) 256e260.
[14] P.J. Simpson, R. Tjossem, A.W. Hunt, K.G. Lynn, V. Munne, Superfast timing performance from ZnO scintillators, Nucl. Instrum. Methods Phys. Res. Sect. A Accel. Spectrom. Detect. Assoc. Equip. 505 (2003) 82e84.
[15] P.A. Rodnyi, I.V. Khodyuk, Optical and luminescence properties of zinc oxide (Review), Optic Spectrosc. 111 (2011) 776e785.
[16] Ü. Özgür, et al., A comprehensive review of ZnO materials and devices, J. Appl. Phys. 98 (2005), 041301.
[17] Z.L. Wang, ZnO nanowire and nanobelt platform for nanotechnology, Mater. Sci. Eng. R Rep. 64 (2009) 33e71.
[18] H. Liu, Z. Feng, J. Wang, J. Diao, D. Su, Synthesis of hollow carbon nano-structures using a ZnO template method, N. Carbon Mater. 31 (2016) 87e91.
[19] K. Liu, M. Sakurai, M. Liao, M. Aono, Giant improvement of the performance of ZnO nanowire photodetectors by Au nanoparticles, J. Phys. Chem. C 114 (2010) 19835e19839.
[20] E. Butanovs, et al., Fast-response single-nanowire photodetector based on ZnO/WS2 core/shell heterostructures, ACS Appl. Mater. Interfaces 10 (2018) 13869e13876.
[21] A. Pescaglini, et al., Hot-electron injection in Au nanorodeZnO nanowire hybrid device for near-infrared photodetection, Nano Lett. 14 (2014) 6202e6209.
[22] O. Lupan, V. Postica, T. Pauporte, M. Hoppe, R. Adelung, UV nano-photodetectors: a case study of individual Au-modified ZnO nanowires, Sensor Actuator Phys. 296 (2019) 400e408.
[23] J. Grottrup,€ et al., UV detection properties of hybrid ZnO tetrapod 3-D net-works, Vacuum 146 (2017) 492e500.
[24] H.-M. Kim, J.-H. Park, S.-K. Lee, Fiber optic sensor based on ZnO nanowires decorated by Au nanoparticles for improved plasmonic biosensor, Sci. Rep. 9 (2019) 15605.
[25] J. Zhang, et al., Layered ultrathin PbI2 single crystals for high sensitivity flexible photodetectors, J. Mater. Chem. C 3 (2015) 4402e4406.
[26] Y. Fu, et al., Metal halide perovskite nanostructures for optoelectronic appli-cations and the study of physical properties, Nat. Rev. Mater. 4 (2019) 169e188.
[27] H.L. Zhu, et al., Achieving high-quality SnePb perovskite films on comple-mentary metal-oxide-semiconductor-compatible metal/silicon substrates for efficient imaging array, ACS Nano 13 (2019) 11800e11808.
[28] H.L. Zhu, et al., Low-bandgap methylammonium-rubidium cation Sn-rich perovskites for efficient ultraviolet-visible-near infrared photodetectors, Adv. Funct. Mater. 28 (2018) 1706068.
[29] H.L. Zhu, et al., Room-temperature solution-processed NiOx:PbI2 nano-composite structures for realizing high-performance perovskite photodetec-tors, ACS Nano 10 (2016) 6808e6815.
[30] F. Ye, et al., High-quality cuboid CH3NH3PbI3 single crystals for high perfor-mance X-ray and photon detectors, Adv. Funct. Mater. 29 (2019) 1806984.
[31] K. Shah, et al., Lead iodide X-ray detection systems, Nucl. Instrum. Methods Phys. Res. Sect. A Accel. Spectrom. Detect. Assoc. Equip. 380 (1996) 266e270.
[32] J.F. Condeles, et al., Fabrication and characterization of thin films of PbI2 for medical imaging, J. Non-Cryst. Solids 338e340 (2004) 81e85.
[33] X.H. Zhu, Z.R. Wei, Y.R. Jin, A.P. Xiang, Growth and characterization of a PbI2 single crystal used for gamma ray detectors, Cryst. Res. Technol. 42 (2007) 456e459.
[34] H. Sun, et al., Laser-induced surface recrystallization of polycrystalline PbI2 thick films for X-ray detector application, Appl. Surf. Sci. 427 (2018) 1146e1151.
[35] M. Zhong, et al., Large-scale 2D PbI2 monolayers: experimental realization and their indirect band-gap related properties, Nanoscale 9 (2017) 3736e3741.
[36] D.L. Duong, S.J. Yun, Y.H. Lee, van der Waals layered materials: opportunities and challenges, ACS Nano 11 (2017) 11803e11830.
[37] W. Choi, et al., Recent development of two-dimensional transition metal dichalcogenides and their applications, Mater. Today 20 (2017) 116e130.

[38] A.S. Toulouse, et al., Frenkel-like Wannier-Mott excitons in few-layer PbI2, Phys. Rev. B 91 (2015) 165308.
[39] A. Splendiani, et al., Emerging photoluminescence in monolayer MoS2, Nano Lett. 10 (2010) 1271e1275.
[40] M. Zhong, et al., Flexible photodetectors based on phase dependent PbI2 single crystals, J. Mater. Chem. C 4 (2016) 6492e6499.
[41] W. Zheng, et al., High-crystalline 2D layered PbI2 with ultrasmooth surface: liquid-phase synthesis and application of high-speed photon detection, Adv. Electron. Mater. 2 (2016) 1600291.
[42] Y. Wang, L. Gan, J. Chen, R. Yang, T. Zhai, Achieving highly uniform two-dimensional PbI2 flakes for photodetectors via space confined physical va-por deposition, Sci. Bull. 62 (2017) 1654e1662.
[43] J. Liu, et al., Synthesis of PbI2 nanowires for high sensitivity photodetectors, RSC Adv. 6 (2016) 59445e59449.
[44] J. Zhang, et al., Low-temperature heteroepitaxy of 2D PbI 2/graphene for large-area flexible photodetectors, Adv. Mater. 30 (2018) 1803194.
[45] B. Polyakov, et al., Unexpected epitaxial growth of a few WS2 layers on {1100} facets of ZnO nanowires, J. Phys. Chem. C 120 (2016) 21451e21459.
[46] E. Butanovs, A. Kuzmin, J. Butikova, S. Vlassov, B. Polyakov, Synthesis and characterization of ZnO/ZnS/MoS2 core-shell nanowires, J. Cryst. Growth 459 (2017) 100e104.
[47] F. Chen, T. Wang, L. Wang, X. Ji, Q. Zhang, Improved light emission of MoS2 monolayers by constructing AlN/MoS2 coreeshell nanowires, J. Mater. Chem. C 5 (2017) 10225e10230.
[48] Z. Fan, et al., Toward the development of printable nanowire electronics and sensors, Adv. Mater. 21 (2009) 3730e3743.
[49] M. Kobayashi, et al., Development of vertically aligned ZnO-nanowires scin-tillators for high spatial resolution x-ray imaging, Appl. Phys. Lett. 106 (2015), 081909.
[50] A. Taheri, S. Saramad, S. Setayeshi, ZnO nanowires in polycarbonate mem-brane as a high resolution X-ray detector (a Geant4 simulation), Nucl. Instrum. Methods Phys. Res. Sect. A Accel. Spectrom. Detect. Assoc. Equip. 716 (2013) 15e22.
[51] J. Wallentin, et al., Hard X-ray detection using a single 100 nm diameter nanowire, Nano Lett. 14 (2014) 7071e7076.
[52] J. Wallentin, M. Osterhoff, T. Salditt, In operando X-ray nanodiffraction reveals electrically induced bending and lattice contraction in a single nanowire de-vice, Adv. Mater. 28 (2016) 1788e1792.
[53] A. Johannes, et al., In operando X-ray imaging of nanoscale devices: compo-sition, valence, and internal electrical fields, Sci. Adv. 3 (2017) eaao4044.
[54] P. Yang, et al., Controlled growth of ZnO nanowires and their optical prop-erties, Adv. Funct. Mater. 12 (2002) 323.
[55] J. Heyd, G.E. Scuseria, M. Ernzerhof, Hybrid functionals based on a screened Coulomb potential, J. Chem. Phys. 118 (2003) 8207e8215.
[56] R. Dovesi, et al., Quantum-mechanical condensed matter simulations with CRYSTAL, Wiley Interdiscipl. Rev. Comput. Mol. Sci. 8 (2018), e1360.
[57] H.J. Monkhorst, J.D. Pack, Special points for Brillouin-zone integrations, Phys. Rev. B 13 (1976) 5188e5192.
[58] J.F. Condeles, R.A. Ando, M. Mulato, Optical and structural properties of PbI2 thin films, J. Mater. Sci. 43 (2008) 525e529.
[59] C. Lan, et al., Large-scale synthesis of freestanding layer-structured PbI2 and MAPbI3 nanosheets for high-performance photodetection, Adv. Mater. 29 (2017) 1702759.
[60] C.S. Lao, et al., ZnO nanobelt/nanowire Schottky diodes formed by dielec-trophoresis alignment across Au electrodes, Nano Lett. 6 (2006) 263e266.
[61] T. Zhai, et al., Recent developments in one-dimensional inorganic nano-structures for photodetectors, Adv. Funct. Mater. 20 (2010) 4233e4248.
[62] G. Cheng, et al., ZnO nanowire Schottky barrier ultraviolet photodetector with high sensitivity and fast recovery speed, Appl. Phys. Lett. 99 (2011) 203105.
[63] B. Mallampati, S.V. Nair, H.E. Ruda, U. Philipose, Role of surface in high photoconductive gain measured in ZnO nanowire-based photodetector, J. Nanoparticle Res. 17 (2015) 176.
[64] J.-M. Wu, C.-H. Kuo, Ultraviolet photodetectors made from SnO2 nanowires, Thin Solid Films 517 (2009) 3870e3873.
[65] N. Yamazoe, J. Fuchigami, M. Kishikawa, T. Seiyama, Interactions of tin oxide surface with O2, H2O AND H2, Surf. Sci. 86 (1979) 335e344.
[66] S.C. Chang, Oxygen chemisorption on tin oxide: correlation between electrical conductivity and epr measurements, J. Vac. Sci. Technol. 17 (1979) 366e369.

Institute of Solid State Physics, University of Latvia as the Center of Excellence has received funding from the European Union's Horizon 2020 Framework Programme H2020-WIDESPREAD-01-2016-2017-TeamingPhase2 under grant agreement No. 739508, project CAMART²